



ELSEVIER

Available online at www.sciencedirect.com

 ScienceDirect

Proceedings of the Combustion Institute 31 (2007) 1345–1352

Proceedings
of the
Combustion
Institute

www.elsevier.com/locate/proci

Fractal characterisation of high-pressure and hydrogen-enriched CH₄–air turbulent premixed flames

Cécile Cohé^{a,*}, Fabien Halter^a, Christian Chauveau^a,
Iskender Gökalp^a, Ömer L. Gülder^b

^a *Laboratoire de Combustion et Système Réactifs, Centre National de la Recherche Scientifique,
1C, avenue de la Recherche Scientifique, 45071 Orléans Cedex 2, France*

^b *University of Toronto, Institute for Aerospace Studies, 4925 Dufferin Street, Toronto, Ont., Canada M3H 5T6*

Abstract

Flame surface characteristics were measured in turbulent premixed flames of hydrogen-enriched methane–air mixtures at elevated pressures. The equivalence ratio range was from 0.6 to 0.8 and the hydrogen mole fraction in the fuel was varied from 0 to 0.2. The pressure range covered from atmospheric to 0.9 MPa. Planar Mie scattering measurements were performed to obtain the flame front images, which were further analyzed for fractal parameters, flame front curvature statistics, and flame surface density. Non-dimensional turbulence intensity, u'/S_L , changed in proportion to the pressure and was 1.53 at atmospheric pressure and 6.51 at 0.9 MPa. With increasing pressure the flame images displayed finer structures indicating that the flame surface area was increasing with pressure. This was also indicated by the probability density function of the flame front curvature as a function of the pressure. Fractal dimension showed a strong dependence on pressure and increased from about 2.1 at atmospheric pressure to about 2.25 at 0.9 MPa. Fractal parameters, including inner and outer cut-offs, agree to a certain extent with the previous experimental data obtained at atmospheric and elevated pressures. The sensitivity of the fractal dimension to u'/S_L was found to depend on the way u'/S_L was varied. A strong correlation between the inner cut-off scale and the average flame radius of curvature was demonstrated. The implications of these results for flame surface density estimations are discussed.

© 2006 The Combustion Institute. Published by Elsevier Inc. All rights reserved.

Keywords: Premixed turbulent combustion; High-pressure premixed turbulent flames; Hydrogen-enriched methane flames; Fractal characteristics of premixed flames; Surface density of high-pressure flames

1. Introduction

Lean premixed combustion is currently one of the most promising concepts for substantial reduction of gas turbine emissions while maintaining high efficiency. However, some of the benefits

of lean premixed combustion are offset by the inherent problems of flame stability and flammability limits. Hydrogen enrichment of lean premixed combustion of natural gas is a potential solution to these problems.

Our understanding of the dynamics and flame surface characteristics of lean premixed and hydrogen-enriched methane combustion at elevated pressures is extremely limited [1–5]. One of the sub-grid scale models widely used in large eddy

* Corresponding author. Fax: +33 0 2 38 25 60 04.
E-mail address: cohe@cnsr-orleans.fr (C. Cohé).

simulation of premixed turbulent flames is the power-law approach. These are based on the flamelet models in which the chemical reactions are assumed to take place in thin layers, separating fresh gases from burned products, being wrinkled by the turbulence. One of the most common approaches to model the flamelet surface area is to use power-law relationships based on the fractal nature of the turbulent flame surfaces. This approach requires knowledge about the fractal parameters, that are fractal dimension, and inner and outer cut-offs which are not available for high-pressure premixed and hydrogen-enriched methane flames. Even, there exists some controversies at atmospheric conditions regarding the sensitivity of the fractal dimension to turbulence characteristics [1,6–10].

In this work, flame surface characteristics are measured in conical (Bunsen type) turbulent premixed flames of hydrogen-enriched methane–air mixtures at elevated pressures. The ranges of equivalence ratios and hydrogen mole fractions in fuel were 0.6–0.8 and 0–0.2, respectively. The pressure range covered was from atmospheric to 0.9 MPa. Non-dimensional turbulence intensity u'/S_L was 1.53 at atmospheric pressure and 6.51 at 0.9 MPa. The main objective of the investigation was to determine the effects of high-pressure and hydrogen addition on the fractal parameters. The behaviour of fractal parameters with the turbulence dynamic range variation can be investigated by increasing the pressure which induces smaller turbulence scales. At a constant turbulence intensity, u' , the non-dimensional turbulence intensity, u'/S_L , can be changed either by changing the pressure (which changes the turbulence scale range) or by changing the fresh mixture composition (by changing the equivalence ratio or the hydrogen mole fraction in the fuel). With this, it is possible to investigate whether the sensitivity of fractal parameters to non-dimensional turbulence intensity depends on the way u'/S_L is changed.

In the following sections of the paper, the experimental methodology and the fractal analysis are first presented. The results section comprises the discussion of the fractal dimension and cut-off scales with varying parameters. The last section focuses on the implications of the current findings on the estimation of flame surface density in turbulent premixed flames.

2. Experimental methodology

2.1. The combustion chamber

The stainless steel cylindrical combustion chamber [2] can sustain premixed turbulent flames up to 1 MPa pressure. The chamber consists of two cylindrical halves of 600 mm high, each equipped with four windows of 100 mm diameter

for optical diagnostics. The internal chamber diameter is 300 mm and the chamber volume is about 80 L. Water flows through the wall jackets for cooling the chamber. The central burner can be moved along the chamber vertical z -axis by means of a stepping motor. The chamber internal walls are painted black with a laser light absorbing paint resistant to high temperatures. Electrical resistance heaters keep the windows free from water condensation. A nitrogen flow is able to dry the windows during measurements if necessary. The internal pressure is set automatically using an electrical valve piloted by a PID controller. A pressure gauge and a thermocouple are used to check the internal burnt gas pressure and temperature.

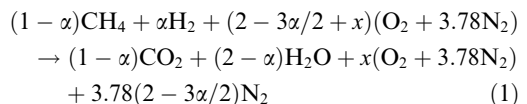
2.2. The burner

The burner [2] is a classical axisymmetric turbulent Bunsen burner designed for premixed flame experiments. The internal burner diameter and length are, respectively 25 and 230 mm. A perforated plate is located 50 mm upstream of the burner exit and generates the cold flow turbulence. An annular laminar stoichiometric methane–air pilot flame stabilizes the turbulent main flame. The translation system supporting the optical diagnostics can move along the transverse x -axis with an accuracy of 0.1 mm. Dry air is provided to the premixer by a 1.3 MPa compressor and is cleaned by a sub-micron filter. Methane and hydrogen are supplied by compressed gas bottles. All flows are controlled by regulated thermal mass flowmeters.

2.3. Mixture and experimental conditions

During the experiments, the bulk mean flow velocity, U , is kept constant at 2.1 m/s for all pressure and mixture conditions. This means that the mass flow rate increases proportionally with the pressure. The pilot flame flow corresponds to approximately 7% of the main flow rate. Turbulence is generated by a perforated plate of 2.5 mm diameter holes arranged in a hexagonal array; its blockage ratio is 0.51.

The overall combustion reaction for $\text{CH}_4 + \text{H}_2 + \text{air}$ mixtures can be written as



where x is the excess air parameter, α is the hydrogen mole fraction in the fuel ($\text{CH}_4 + \text{H}_2$). When the percentage of hydrogen in the fuel is changed, the methane concentration is adjusted to keep constant the global equivalence ratio. Methane–hydrogen–air turbulent premixed flames are investigated for the following ranges of the main

Table 1
Experimental conditions and fractal analysis results

P (MPa)	ϕ	α	u' (m/s)	S_L (m/s)	u'/S_L	Lu (mm)	η (mm)	δ_L (mm)	Re_{Lu}	D_3	ε_i (mm)	ε_0 (mm)	R_{Cav} (mm)	$A1$	$A2$
0.1	0.6	0	0.17	0.112	1.53	3.0	0.22	0.20	32	2.097	1.5	14	4.20	1.49	3.9
0.3	0.6	0	0.19	0.058	3.23	3.1	0.09	0.13	115	2.209	0.85	9	3.01	1.68	6.37
0.5	0.6	0	0.18	0.041	4.39	2.9	0.06	0.11	177	2.241	0.8	8	2.46	1.72	7.12
0.7	0.6	0	0.19	0.034	5.54	3.0	0.05	0.10	249	2.248	0.75	6.5	2.54	1.72	8.73
0.9	0.6	0	0.19	0.029	6.51	3.1	0.04	0.09	341	2.250	0.7	6	2.35	1.74	9.61
0.1	0.7	0	0.17	0.189	0.91	3.0	0.22	0.12	34	2.134	1.3	8.5	3.90	1.48	4.81
0.1	0.8	0	0.17	0.266	0.64	3.0	0.22	0.08	34	2.139	1.1	4.5	3.31	1.47	5
0.1	0.6	0.1	0.17	0.121	1.44	3.0	0.22	0.19	33	2.101	1.3	7	3.70	1.84	3.23
0.1	0.6	0.2	0.18	0.132	1.33	3.0	0.22	0.18	32	2.112	1.2	6	3.50	2.04	3.31

parameters: $\alpha = 0, 0.1, 0.2$; $P = 0.1\text{--}0.9$ MPa; $\Phi = 0.6, 0.7, 0.8$ (see also Table 1).

2.4. Mie scattering tomography

A 15 Hz pulsed Nd–Yag laser (Spectra Physics GCR 130) at 532.5 nm is used for laser Mie scattering flame tomography. The pulse energy is 180 mJ. The laser beam passing through a 1000 mm focal length spherical lens and a 25.4 mm focal length cylindrical lens produces a light sheet 200 μm thick and approximately 100 mm high.

The flow is seeded by olive oil droplets supplied by an atomizer. The mean droplet diameter is equal to 3.3 μm at atmospheric pressure, as determined by PDPA technique. The Mie scattered light is collected at 90° to the sheet by a CDD camera (TSI PIV CAM 10–30, 1016 \times 1008 pixels²). The overall resolution is 0.11 mm/pixel. Three series of 300 images are obtained for each experimental condition. Typical binarised tomographic images for three different pressures, three hydrogen mole fractions and three different equivalence ratios are shown in Fig. 1 to illustrate the global effect of the parameter varied, whereas the two others are held constant.

For constant mixture composition and equivalence ratio, increasing the pressure generates smaller flame elements [2–4]. It was shown previously by LDA measurements in the reactants flow [2] that the pressure increase does not affect the turbulent kinetic energy and the integral length scale when the bulk mean exit velocity is kept constant. However, due to the reduction of the kinematic viscosity with pressure and the consequent increase of the turbulent Reynolds number, the dynamic range of the turbulent scales increases with the promotion of the generation of smaller scale eddies that decrease Taylor and Kolmogorov scales (see Table 1). Therefore, with increasing pressure, the flame surface density increases significantly [2]. At atmospheric pressure, increasing the equivalence ratio (on the lean side) or the hydro-

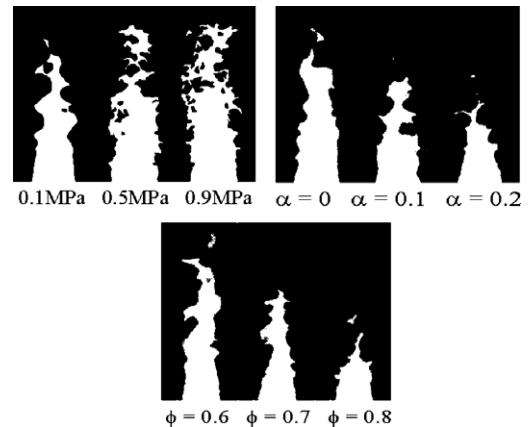


Fig. 1. Instantaneous tomographic flame images for three different pressures ($\alpha = 0, \phi = 0.6$), for three different H_2 enrichments ($P = 0.1$ MPa, $\phi = 0.6$) and three different equivalence ratios ($P = 0.1$ MPa, $\alpha = 0$).

gen mole fraction have similar effects (Fig. 1), i.e. reducing the total flame length at constant reactants bulk velocity, indicating therefore increased mixture reactivity. It should be recalled that the laminar propagation velocity decreases strongly with increasing pressure, but increases with increasing equivalence ratio (on the lean side) or with increasing hydrogen mole fraction [5].

In Ref. [2], the pressure effect on the structure of turbulent methane–air flames was investigated in detail. It was shown that all the topographic parameters of the instantaneous flame fronts and their averaged values (flamelet wrinkling scale, curvature and orientation angle and the flame surface density) vary quasi-linearly with the square-root of the turbulent Reynolds number based on the integral length scale, $(Re_{Lu})^{1/2}$. This scaling with $(Re_{Lu})^{1/2}$ indicates that the flame structure is responding to the dynamic range of the turbulent scales. It was also remarked that studying high-pressure turbulent premixed flames gives a unique opportunity to explore the small scale

effects on turbulent flames while keeping all other parameters constant (including the integral length scale, and mean and fluctuating velocities). It was therefore decided to pursue this investigation using the fractal approach to confirm the previous conclusions and also to quantitatively document the variation of the fractal parameters of turbulent premixed flames with turbulence and flame conditions.

3. Image processing and fractal analysis

The spatial resolution of the imaging system and image processing method can influence the determination of fractal parameters [11]. In this work, Mie scattering images were binarised with a threshold determined as the minimum value between the two peaks of the pixel intensity probability density distribution. This minimum represents the instantaneous flame front. An edge finding algorithm was then applied to each image. These edges were filtered by a Butterworth filter to remove the digital noise. The filter properties were chosen to conserve flame structures larger or equal to 1 mm, which correspond to the dimension of the instantaneous total flame front thickness. From the filtered edges, the binarised images without noise due to pixellisation were reconstructed. The fractal analysis was carried out on filtered edges and the reconstructed binarised images.

The fractal dimension D_2 was obtained by the Richardson–Mandelbrot approach, applied to the two-dimensional tomography images. This approach was also used in several previous studies. Since the instantaneous flame fronts are continuous, the caliper stepping method was chosen in this work. Considering a compass spacing ε , the length along the flame front can be defined as $L(\varepsilon) = N(\varepsilon) \cdot \varepsilon$, where N is the number of steps necessary to cover the whole the flame front. Figure 2 represents the evolution of $\log(L(\varepsilon))$ versus $\log(\varepsilon)$, by averaging 300 images. The fractal dimension is then determined from the slope m of the linear part of each curve as $D_2 = 1 - m$. The three-dimensional fractal dimension D_3 is considered to be equal to $D_2 + 1$. Fractal dimensions obtained from individual fractal curves are similar to those from average fractal curves [8]. For an ideal fractal behaviour, the double-log plot of L versus ε should be linear. However, in practice, the linear slope is only available between the inner cut-off scale ε_i and the outer cut-off scale ε_0 . The fractal self-similarity exists in between these two limits. For two-dimensional images, the fractal dimension of the edge is given by

$$\frac{L_{\varepsilon_i}}{L_{\varepsilon_0}} = \left(\frac{\varepsilon_0}{\varepsilon_i} \right)^{D_2-1} \quad (2)$$

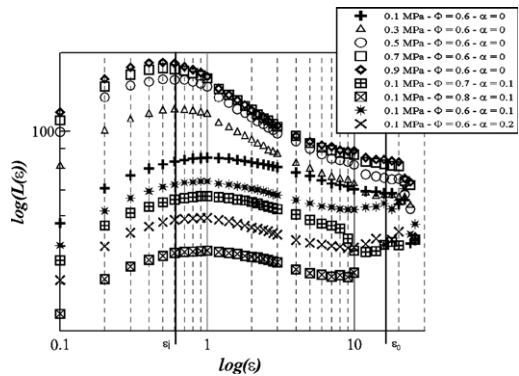


Fig. 2. Average flame length as a function of scale from 300 images at different pressures. $L(\varepsilon)$ and ε are in mm.

For the work reported here, the fractal parameters were determined from data sets, each set containing about 300 images, for better accuracy. The fractal dimension uncertainties do not exceed 1% of D_3 and for the inner and outer cut-off scale, the uncertainties are, respectively less than 7.5% of ε_i and 12% of ε_0 .

4. Results and discussion

4.1. Fractal dimensions

The fractal analysis results for each investigated flame conditions are summarized in Table 1. Figure 2 shows the evolution of the fractal curves for increasing pressures in the combustion chamber. The increase of the fractal dimension with pressure can be observed from the higher slopes of the linear parts of the fractal curves. It was also observed that the fractal curves are shifted to the left with increasing pressure, indicating smaller cut-off scales. The same phenomenon is observed when the equivalence ratio or the percentage of hydrogen increases. The decrease of the length as ε approaches 0.1 mm is due to the image pixelisation and it is not a physical phenomenon. The maximum error function is equal to $-1/(N+1)$, where N is defined by $\varepsilon = N$ (size of pixel); this is why the flame length is under-evaluated at small ε .

The variation of the fractal dimension D_3 with u'/S_L is shown in Fig. 3 for all conditions summarized in Table 1. Figure 3 clearly shows that the method used to vary the u'/S_L ratio is important. The increasing D_3 part of the curve corresponds to flame conditions with fixed composition and equivalence ratio but increasing pressure. Under these conditions, u' is constant and the increase in u'/S_L is due to a decrease in S_L with pressure [2,3]. In the left part of the curve, D_3 is shown to increase with decreasing u'/S_L ratio. Here, u'

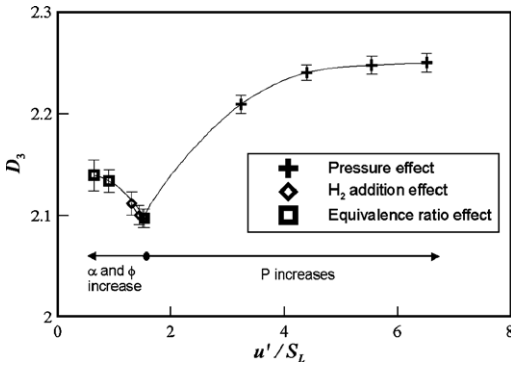


Fig. 3. Fractal dimension D_3 versus u'/S_L for all investigated cases.

is again constant but S_L increases either with H_2 addition or with the increase of the equivalence ratio.

Therefore two different mechanisms of fractal dimension increase are observed. For fixed composition and turbulence intensity, the pressure increase induces a raise in u'/S_L , but also it decreases the small scale turbulence characteristic dimensions generating smaller flame elements and therefore a more fractalized flame contour with increased D_3 . This behaviour is also observed by Kobayashi and Kawazoe [12] in his experiments with a fixed composition and increasing pressure (Fig. 4). Mantzaras et al. [6] also showed that the fractal dimension increases with u'/S_L at high pressures. In Fig. 4, Kobayashi's results are for a perforated plate with hole diameters 1–4 mm, at atmospheric pressure, 0.5 and 1 MPa, for a lean CH_4 /air mixture with an equivalence ratio of 0.9. One can also notice that the fractal dimension determined by Kobayashi is higher than the present results, but both approaching the value of 2.3. This difference can be explained by the higher equivalence ratio of Kobayashi's flames (0.9) whereas the present results are for an equivalence

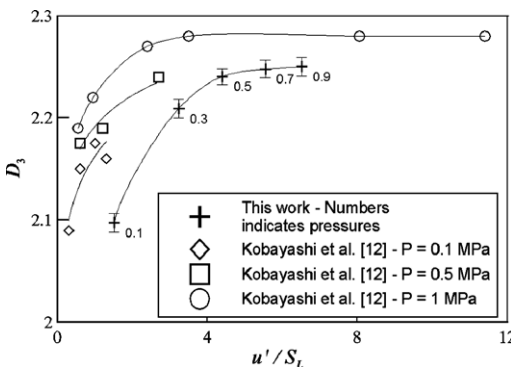


Fig. 4. D_3 versus u'/S_L for different pressures.

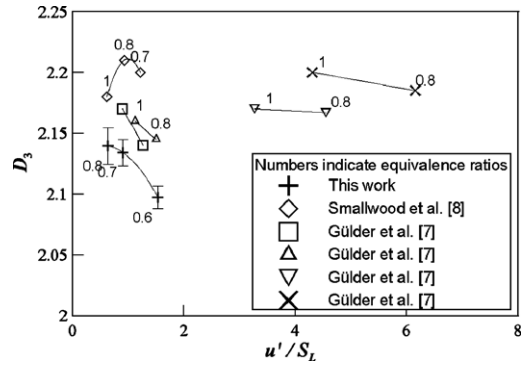


Fig. 5. D_3 versus u'/S_L for different equivalence ratios.

ratio of 0.6 (see below). Since u' and Lu do not change with pressure, the effect of the Reynolds number with increasing pressure is reflected as an increase in the ratio of large scale to small scale turbulence.

For fixed turbulence conditions (the left part of the curve in Fig. 3) and increasing equivalence ratio or hydrogen mole fraction, S_L increases, u'/S_L decreases, but D_3 increases. This behaviour is also clearly observed in other experiments in the literature, such as those shown in Fig. 5, and taken from Gülder et al. [1] and Smallwood et al. [8]. The results presented here from these references correspond to constant integral length scales, with values comparable to ours (between 1.5 and 3 mm, depending on the turbulence generators used).

It should be noted that for flame parameters variations through the equivalence ratio increase from 0.6 to 0.8 or hydrogen addition, the instantaneous flame front thickness decreases (see Table 1). Therefore, even if the turbulence scale dynamics is not changing (contrary to the changes induced by the pressure increase), a larger fraction of the small scale end of the turbulence spectrum contributes to wrinkle the instantaneous flame fronts, thus increasing (albeit moderately) their fractalization.

These results indicate a significant role of turbulent length scales in the fractalization of premixed turbulent flames rather than a sole dominant role of the u'/S_L ratio. This analysis also predicts that if the u'/S_L ratio is to be increased without changing either the turbulence scale range or the flamelet thickness, there should be no change in the fractal characteristics of turbulent premixed flames.

4.2. Inner cut-off scale

Several authors have suggested generalized correlations for the inner cut-off. For example Gülder and Smallwood [7] and Roberts et al. [9]

propose a linear relationship between the normalised inner cut-off scale ε_i/δ_L and $Ka^{-1/2}$. The Gibson scale is also proposed to scale with the inner cut-off [13]. The inner cut-off scales determined in the present study are compared to those from the previously cited works [1,8,12], when the pressure and the equivalence ratios change. Figures 7 and 8 present the variation of ε_i versus u'/S_L . Similarly to the variation of D_3 , two different patterns are observed depending on how the u'/S_L ratio is varied. In Fig. 6, with increasing pressure at fixed mixture composition, ε_i decreases with increasing u'/S_L , both for the present results and those of Kobayashi [4,12]. As for D_3 , the dominant effect here is the reduction of turbulence scales with pressure and the consequent generation of small scale flame elements. The opposite behaviour is shown on Fig. 7 when u'/S_L is increased by decreasing S_L . In this case, the inner cut-off scale increases with increasing u'/S_L . This is because of the thickening of the instantaneous flame fronts with decreasing S_L and the reduced efficiency of small scale turbulence elements to wrinkle them.

In Table 1, the laminar flame thickness δ_L is given by the Zeldovich definition and is computed with the PREMIX code from the program package CHEMKIN-II. The chemical kinetics was modelled by GRI-Mech v.3.0 truncated by eliminating the sub mechanism for N_2 oxidation. The mixture average formulation without thermal diffusion was used in the transport model. The computations performed with and without the thermal diffusion term were very similar. First, we have observed a quasi-constant ratio between the inner cut-off scale and the instantaneous flame front thickness when the pressure is varied for fixed mixture composition and equivalence ratio. From Table 1, the average value of ε_i/δ_L is found equal to 7.3 from the atmospheric pressure to 0.9 MPa. When the pressure is kept constant and the equivalence ratio is varied from 0.6 to 0.8, ε_i/δ_L increases from 7.5 to 13.8. Finally, when the hydrogen

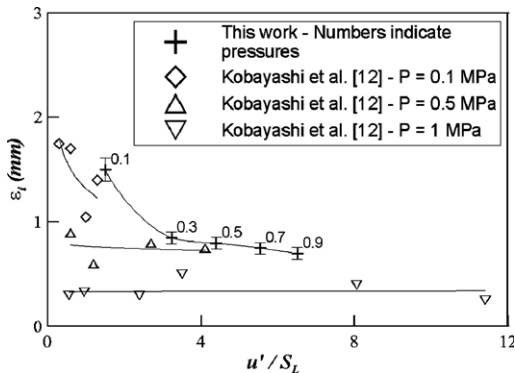


Fig. 6. Inner cut-off scale versus u'/S_L for different pressures.

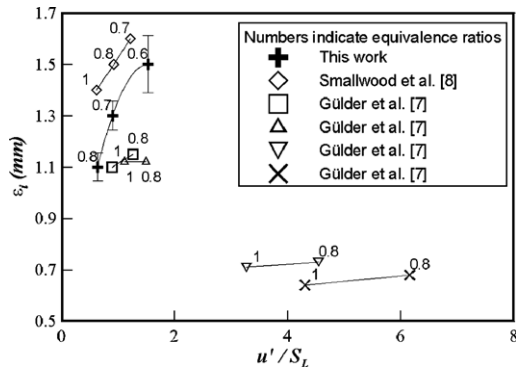


Fig. 7. Inner cut-off scale versus u'/S_L for different equivalence ratios.

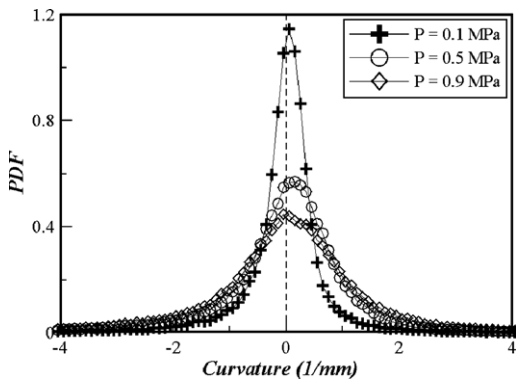


Fig. 8. Pdf of curvature for different pressures.

mole fraction in the fuel is increased from 0 to 0.2, ε_i/δ_L decreases from 7.5 to 6.7. Therefore, the variation of ε_i/δ_L is complex and depends both on the turbulence structure and the fundamental flame propagation velocity.

This strong dependency between the inner cut-off and the characteristic flame and turbulence scales indicates also a strong correlation between the inner cut-off scale and the global topography of the flame as depicted for example by the average flame curvature or the average flame radius of curvature. This idea was also introduced in [10].

Figure 8 illustrates the distribution of experimental curvatures for different pressures at fixed mixture composition and equivalence ratio. The local curvature h is estimated for each pixel along the filtered flame contour with

$$h = \frac{\dot{x} \cdot \ddot{y} - \ddot{x} \cdot \dot{y}}{(\dot{x}^2 + \dot{y}^2)^{3/2}} \quad (3)$$

where $x(s)$ and $y(s)$ are the orthogonal coordinates and s is the curvilinear abscissa. It is observed that the curvature increases with pressure, in agreement with the enhancement of the small scale

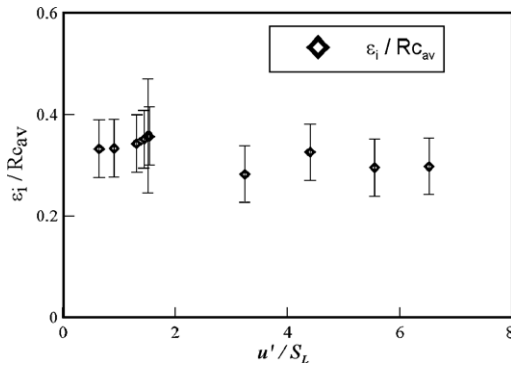


Fig. 9. Ratio between the inner cut-off scale and the mean radius of curvature versus u'/S_L .

turbulence with pressure. The mean radii of curvature R_{cav} , are determined for each average flame (see Table 1). Figure 9 shows the ratio of the inner cut-off to the mean radius of curvature versus u'/S_L . This ratio is constant around a value of 0.33. The flame front average curvature or the average radius of curvature depends both on the turbulence length scales and the flame propagation velocity. Therefore, as shown on Fig. 9, the ratio ε_i/R_{cav} captures globally the relationship between the inner cut-off scale and the chemical and turbulence parameters of the mixture. In addition, it has been shown in Ref. [2] that the variance of flame front curvature scales linearly with $(Re_{Lu})^{1/2}$, that is with the ratio between the large and small turbulence length scales. Therefore, the present experimental results and analysis reinforce the approach proposed in [10] where it is suggested to model the flame wrinkling parameter using a fractal approach and furthermore to model the inner cut-off as the inverse surface averaged curvature of the flame. However, the assumption of a monotonic increase of the fractal dimension D_3 with u'/S_L adopted in [10] is not supported by the present experimental results and analysis.

4.3. Outer cut-off scale

Measured outer cut-off scales are presented on Table 1. At atmospheric pressure they increase with u'/S_L varied by decreasing the equivalence ratio; as also observed in [8]. The smallest ε_0 value is larger than the measured integral length scale (3 mm); the largest value is about the burner radius (12.5 mm). As shown on Table 1, the outer cut-off scale decreases when pressure increases, paralleling the variation of the inner cut-off scale.

4.4. Flame surface density

As the present numerical computational codes allow the accurate estimate of both the reactants

flow structure and the laminar flame properties, an interesting avenue seems opened up to estimate the flame surface density Σ using its relationship to the fractal characteristics of turbulent premixed flames, such as

$$\int \Sigma dV = S_T/S_L = A(\varepsilon_0/\varepsilon_i)^{D_3-2} \quad (4)$$

For conical flames, it has been shown in Ref. [8] that the above relation can be written as

$$\frac{S_T}{S_L} = \frac{A_{C_{0.5}}}{A_{C_{0.05}}} \left(\frac{\varepsilon_0}{\varepsilon_i} \right)^{D_3-2} \quad (5)$$

where $A_{C_{0.5}}/A_{C_{0.05}}$ represents the ratio between the average flame surface area below the $\langle C \rangle = 0.5$ contour and the one below the $\langle C \rangle = 0.05$ contour. $\langle C \rangle$ is the average progress variable evaluated from the averaged Mie scattering tomography images [2]. The constant $A_{C_{0.5}}/A_{C_{0.05}}$ ratio is displayed in Table 1 as $A1$ and shows values of the order of unity as in [8].

The same constant can also be evaluated using the values of S_T/S_L . In this ratio, the laminar burning velocity is calculated with the CHEMKIN-II package as for the laminar flame thickness; the turbulent burning velocity is obtained with the cone method [14]. The turbulent burning velocity is defined relative to the reactants using as reference the cone corresponding to $\langle C \rangle = 0.1$. The expression of the turbulent burning velocity is therefore

$$S_T = \sqrt{\frac{U^2}{1 + (H/R)^2}} \quad (6)$$

where U is the bulk flow velocity equal to 2.1 m/s for all the investigated cases, R the burner radius of 12.5 mm and H the height of the cone for $\langle C \rangle = 0.1$ for each flame condition. The constant A of Eq. (5) estimated using the S_T/S_L ratio is displayed as $A2$ in Table 1. Its values are larger than $A1$ and lie between 3 and 10. Also, when the S_T/S_L ratio is estimated as $\delta_T \Sigma$ [11], similar values of A as $A2$ are obtained. It is therefore obvious that additional work is needed to establish the relationship between the fractal interpretation of the burning rate for turbulent premixed flames and that based on flame surface density approaches.

5. Conclusions

Flame surface characteristics were measured in turbulent premixed flames of hydrogen-enriched methane–air mixtures from atmospheric to 0.9 MPa pressure. Hydrogen mole fraction in the fuel was from 0 to 0.2, and the equivalence ratio varied from 0.6 to 0.8. We used planar Mie scattering measurements to obtain the flame front

images, which were further analyzed for fractal parameters, flame front curvature statistics, and flame surface density. Non-dimensional turbulence intensity, u'/S_L , changed in proportion to the pressure and was 1.53 at atmospheric pressure and 6.51 at 0.9 MPa.

With increasing pressure the flame images displayed finer structures indicating that the flame surface area was increasing with pressure. This observation was further supported by the observed increase in flame front curvature as the pressure was increased.

Fractal dimension showed a strong dependence on pressure and increased from about 2.1 at atmospheric pressure to about 2.25 at 0.9 MPa. However, sensitivity of the fractal dimension to non-dimensional turbulence intensity was dependent on whether u'/S_L was changed at constant pressure, or u'/S_L was changed as a result of the pressure change. We demonstrated that a strong correlation exists between the inner cut-off scale and the average flame radius of curvature.

Finally, our results point to a significant role of turbulent length scales in the fractalization of premixed turbulent flames rather than a sole dominant role of the u'/S_L ratio.

Acknowledgments

This work was supported by Centre National de la Recherche Scientifique, Conseil Regional Centre, European Commission AFTUR project (Alternative Fuels for Industrial Gas Turbines), Contrat ENK5-CT-2002-0062. C.C. and F.H. are supported by joint Grants from the CNRS

and the Conseil Regional Centre. Ö.L.G. acknowledges financial support by NSERC through a CRO Grant.

References

- [1] Ö.L. Gülder et al., *Combust. Flame* 120 (2000) 407–416.
- [2] T. Lachaux, F. Halter, C. Chauveau, I. Gökalp, I.G. Shepherd, *Proc. Combust. Inst.* 30 (2005) 819–826.
- [3] F. Halter, *Caractérisation des effets de l'ajout d'hydrogène et de la haute pression dans les flammes turbulentes de prémélanges méthane/air*, PhD Thesis, University of Orléans, France (2005).
- [4] H. Kobayashi, T. Nakashima, T. Tamura, K. Maruta, T. Niioaka, *Combust. Flame* 108 (1997) 104–117.
- [5] F. Halter, C. Chauveau, N. Djedäili-Chaumeix, I. Gökalp, *Proc. Combust. Inst.* 30 (2005) 201–208.
- [6] J. Mantzaras, P.G. Felton, F.V. Bracco, *Combust. Flame* 77 (1989) 295–310.
- [7] Ö.L. Gülder, G.J. Smallwood, *Combust. Flame* 103 (1995) 107–114.
- [8] G.J. Smallwood, Ö.L. Gülder, D.R. Snelling, B.M. Deschamps, I. Gökalp, *Combust. Flame* 101 (1995) 461–470.
- [9] W.L. Roberts, J.F. Driscoll, M.C. Drake, L.P. Goss, *Combust. Flame* 94 (1993) 58–69.
- [10] F. Fureby, *Proc. Combust. Inst.* 30 (2005) 593–601.
- [11] I.G. Shepherd, *Proc. Combust. Inst.* 26 (1996) 373–379.
- [12] H. Kobayashi, H. Kawazoe, *Proc. Combust. Inst.* 28 (2000) 375–382.
- [13] N. Peters, *Proc. Combust. Inst.* 22 (1988) 1231–1239.
- [14] H. Kobayashi, T. Tamura, K. Maruta, T. Niioaka, F.A. Williams, *Proc. Combust. Inst.* 26 (1996) 389–396.